Bottom-up Growth of Epitaxial Graphene on 6H-SiC(0001)

Han Huang,[†] Wei Chen,[†,‡,*] Shi Chen,[†] and Andrew Thye Shen Wee[†,*]

[†]Department of Physics, National University of Singapore, 2 Science Drive 3, 117542, Singapore, and [‡]Department of Chemistry, National University of Singapore, 3 Science Drive 3, 117543, Singapore

ABSTRACT We use *in situ* low temperature scanning tunneling microscopy (STM) to investigate the growth mechanism of epitaxial graphene (EG) thermally grown on Si-terminated 6H-SiC(0001). Our detailed study of the transition from monolayer EG to trilayer EG reveals that EG adopts a bottom-up growth mechanism. The thermal decomposition of one single SiC bilayer underneath the EG layers causes the accumulation of carbon atoms to form a new graphene buffer layer at the EG/SiC interface. Atomically resolved STM images show that the top EG layer is physically continuous across the boundaries between the monolayer and bilayer EG regions and between the bilayer and trilayer EG regions.

KEYWORDS: epitaxial graphene · interfacial graphene · silicon carbide · scanning tunneling microscopy · bottom-up growth

Recently, much attention has been devoted to graphene, a single layer of sp^2-bonded carbon atoms arranged in a two-dimensional honeycomb lattice, due to its many exotic properties[1−8] such as the existence of massless Dirac fermions,[1−3] quantum hall effect at room temperature (RT),[7] gate controlled transport (electron or hole) properties,[4] high charge carrier mobility even at high charge carrier concentration at RT,[3−5] gas sensing at the single molecule level,[6] and long spin relaxation length up to micrometer scale at RT.[8] Single layer or few layer graphene films can be prepared by micromechanical cleavage (MCP)[3,4] or chemical exfoliation from bulk graphite powders,[9,10] thermal decomposition of commercial silicon carbide (SiC) substrates in vacuum[11−13] or under atmospheric pressure conditions,[14] or chemical vapor deposition of hydrocarbons on transition metal substrates such as Ni(111),[15−17] Ir(111),[18,19] and Ru(0001).[20,21] In particular, ultrathin epitaxial graphene (EG) films thermally grown on SiC can be patterned using standard nanolithography methods,[11,12] making it compatible with current semiconductor technology and hence a promising material for future nanoelectronics. However, due to the large lattice mismatch between EG and the underlying SiC substrate, the quality of EG grown on SiC is not comparable to the graphene films obtained *via* the MCP method.[22−24] As such, there is a need to understand the growth mechanism and hence to optimize the growth of high quality and large scale EG films for practical applications. Although the graphitization of SiC was first investigated by Van Bommel *et al.* in 1975,[25] the initial graphitization process is still unclear.[26−30] Unresolved issues include the structure of the interfacial graphene buffer layer between EG and SiC, the EG edge states at the domain boundaries, and the EG growth mechanism. Annealing the SiC substrate at temperatures above 1600 °C can also produce well-aligned carbon nanotubes.[31−33] In this article, *in situ* low temperature scanning tunneling microscopy (LT-STM) is used to study the morphology, atomic structure, and the growth mechanism of EG on 6H-SiC(0001) with thickness from one to three atomic layers. Our results reveal that the top EG layer is physically continuous across the domain boundaries between the monolayer and bilayer EG regions and between the bilayer and trilayer EG regions, suggesting a bottom-up growth mechanism for EG on SiC.

RESULTS AND DISCUSSION

The growth of EG on Si-terminated 6H- or 4H-SiC(0001) involves two sequential processes: (i) High temperature annealing of SiC (~1100 °C) leads to the decomposition of SiC followed by the desorption of Si from the surface and an accumulation of carbon atoms to form a carbon-rich surface layer, referred to variously in the literature as the carbon nanomesh, interfacial graphene, or carbon buffer layer; this layer is identified by a $(6\sqrt{3} \times 6\sqrt{3})R30°$ LEED

*Address correspondence to phycw@nus.edu.sg, phyweets@nus.edu.sg.

Received for review October 23, 2008 and accepted November 20, 2008.

Published online December 4, 2008. 10.1021/nn800711v CCC: $40.75

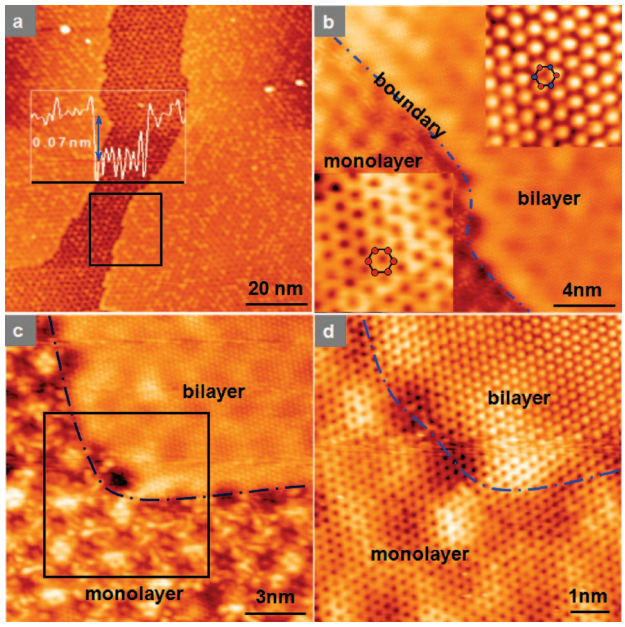

Figure 1. (a) Typical STM image (100 × 100 nm^2, V_T = 1.78 V) of the monolayer (the center darker channel region) and bilayer (the two bright terraces in the right and left part) EG on 6H-SiC(0001); the line profile across the monolayer and the bilayer EG regions is superimposed in panel a. (b) High-resolution STM image (20 × 20 nm^2, V_T = 0.5 V) showing the coexistence of monolayer (lower left part) and bilayer (upper right part) EG; the insets in panel b display the corresponding atomically resolved STM images of monolayer and bilayer EGs, respectively; the red hexagon in the lower left part highlights the hexagonal lattice of the monolayer EG, and the hexagon with alternated red and blue dots in the upper right part represents the two inequivalent triangular sublattices of the bilayer EG. (c) Atomically resolved STM image (15 × 15 nm^2, V_T = 0.5 V) in another region showing the coexistence of the monolayer and bilayer EG and (d) its corresponding detailed image (8 × 8 nm^2, V_T = −0.1 V), as marked by the square in panel c, clearly revealing the physical continuum at the domain boundaries between the monolayer and bilayer EG.

pattern or a 6 × 6 superstructure in STM.[27,34,35] (ii) After annealing at 1200 °C or higher, monolayer (~1200 °C, 2 min), bilayer (~1250 °C, 2 min), or trilayer and thicker (above 1300 °C, 2 min) EG films form on top of the interfacial graphene layer. During the annealing experiments, the chamber pressure was maintained below 5 × 10^{-9} mbar.

Figure 1a shows a typical STM image (100 × 100 nm^2, V_T = 1.78 V) after annealing a 6H-SiC(0001) sample at ~1200 °C. Two bright terraces (left and right parts of the image) are separated by a darker channel. The height difference between the bright (high) and the dark (low) regions is 0.07 ± 0.01 nm, as revealed by the line profile superimposed on this panel. This height difference is much smaller than the SiC bilayer height (0.25 nm) and the interlayer spacing in bulk graphite (0.335 nm). Figure 1b displays a high-resolution STM image (20 × 20 nm^2, V_T = 0.5 V) in another region showing the coexistence of bright (upper right part) and dark (lower left part) regions with 0.07 nm height difference. The dotted curve in Figure 1b delineates the domain boundary separating the bright and dark regions. An atomically resolved STM image (2 × 2 nm^2, V_T = 0.1 V) of the dark (low) region is shown as an inset (lower left inset in Figure 1b), clearly revealing a honeycomb structure highlighted by a hexagon with a lattice constant of 0.24 ± 0.01 nm, in coincidence with the atomic structure of single layer graphene. In contrast, the close-up (2 × 2 nm^2, V_T = 0.1 V) of the bright region (upper right inset) shows a triangular lattice. As previously reported,[36,37] the hexagonal lattice is assigned to monolayer EG and the triangular lattice to bilayer EG, consistent with recent Kelvin probe force microscopy results.[38] The bilayer EG involves AB (Bernal) stacking as in bulk graphite,[39] breaking the symmetry of the graphene hexagonal lattice resulting in two inequivalent sublattices; this leads to the appearance of the triangular lattice in STM imaging. This transition from a hexagonal to triangular lattice is widely used to differentiate monolayer from bilayer or few layer EG on SiC.[40]

It is worth noting that both monolayer EG (dark region) and bilayer EG (bright region) in Figure 1b show a background 6 × 6 contrast modulation, arising from the underlying interfacial graphene with ($6\sqrt{3} \times 6\sqrt{3}$)$R30°$ (or "6 × 6") reconstruction. The attenuation of this 6 × 6 structure is determined by the EG layer thickness.[41] As shown in Figure 1c (15 × 15 nm^2, V_T = 0.5 V), the 6 × 6 superstructure is more apparent in the monolayer EG region (bottom part) and largely attenuated in the bilayer EG region (top part). This is consistent with previous report[36] and further confirms our assignments of monolayer and bilayer EG. The monolayer EG can be better resolved at low tunneling bias voltage conditions. Figure 1d shows the corresponding zoom-in STM image (8 × 8 nm^2), highlighted by the square in Figure 1c. At the low bias condition of V_T = 0.1 V, the honeycomb lattice of monolayer EG is clearly resolved.[42] In particular, the top EG layer is physically continuous from the monolayer EG region to the bilayer EG region since the periodicity of the lattice is continuous across the boundary.

This continuous boundary is a common feature for the transition from monolayer EG to bilayer EG on the same terrace. Panels a and b in Figure 2 are high-resolution STM images (15 × 15 nm^2) taken at very low tip bias voltages (0.05 and −0.05 V, respectively) of the region marked by a black square in Figure 1a. The top graphene layer is clearly continuous across the boundary, which is delineated by the dotted line. On the bilayer EG (right side), a ($\sqrt{3} \times \sqrt{3}$)$R30°$ superstructure, as highlighted in the corresponding detailed image (8 × 4 nm^2) in Figure 2d, appears in the region close to the boundary, as shown in Figure 2a,b. The ($\sqrt{3} \times \sqrt{3}$)$R30°$ superstructure on bilayer EG disappears when imaging at the bias voltages above 0.1 V or below −0.1 V. Figure 2c shows the STM image of the same region but with a larger bias voltage of 0.1 V. The bilayer EG surface is dominated by the typical triangular 1 × 1 lattice, as highlighted in its detailed image

(8×4 nm^2) in Figure 2e. Therefore, the observed ($\sqrt{3} \times \sqrt{3}$)*R*30° superstructure modulation is attributed to an electronic effect, rather than the atomic structure variation. Although the top EG layer is continuous across the boundary from the monolayer EG to the bilayer EG, the interference from electrons scattered at the domain boundaries beneath the top EG layer causes modulation of the electronic structures of the top bilayer EG, leading to the appearance of the ($\sqrt{3} \times \sqrt{3}$)*R*30° superstructure observed at very low bias voltage ($\pm$0.05 V).[43−45]

Figure 3a displays an STM image (150×100 nm^2, $V_T = 1.5$ V) in another region showing the coexistence of monolayer and bilayer EG. The bilayer EG, highlighted in panel a, appears as irregular islands extending from the SiC step edge to the center of the terrace. Figure 3b is the line profile taken along the line AD marked in panel a. The height difference between monolayer and bilayer EG is 0.07 $\pm$ 0.01 nm, measured at point B. Again, the top EG layer is atomically continuous transiting from the bilayer EG to the monolayer EG (data not shown here). It has been reported that the interlayer spacing of EG layers on SiC is 0.34 nm, derived from X-ray reflectivity measurements[46] and first-principles calculations.[29] The 0.07 nm height difference between monolayer and bilayer EG is in good agreement with the value obtained by subtracting the SiC bilayer height (0.25 nm) from the EG interlayer spacing (0.34 nm). As such, we propose a model in Figure 3c to illustrate the atomic structures of neighboring monolayer and bilayer EG. A single SiC bilayer (0.25 nm high) thermally decomposes underneath the interfacial graphene [the ($6\sqrt{3} \times 6\sqrt{3}$)*R*30° reconstruction] of monolayer EG, accompanied by the desorption of Si species from the interface[47] and the release of carbon species to form a new interfacial graphene layer. This leads to the transformation of the original interfacial graphene layer to a new first EG layer atop the newly formed interfacial graphene, thereby resulting in a transition from monolayer to bilayer EG. From this bottom-up growth model, the top EG layers of the neighboring bilayer and monolayer EG remain continuous as they originate from the same EG layer. This explains the observed physical continuum at the boundary between monolayer and bilayer EG, as shown in Figure 1b,d. The lowering of the EG layer due to the decomposition of the underlying SiC bilayer (0.25 nm) is compensated by the formation of a second EG layer with interlayer spacing of 0.34 nm, consistent with the measured height difference between the monolayer and the bilayer EG (*i.e.*, 0.07 $\pm$ 0.01 nm). The surface density of C atoms in a graphene layer (3.82×10^{15} cm^{-2}) is triple that in a SiC bilayer (1.22×10^{15} cm^{-2}), so it requires the consumption of three consecutive SiC bilayers to form a complete graphene layer.[18,29] This is in contrast to our STM observations and the proposed model that require only the thermal decomposition of a single SiC bilayer to form EG. We propose that the decomposition of a single SiC bilayer results in the formation of the new interfacial graphene layer partially covering the decomposition area. More detailed experimental investigations will be carried out to confirm this hypothesis.

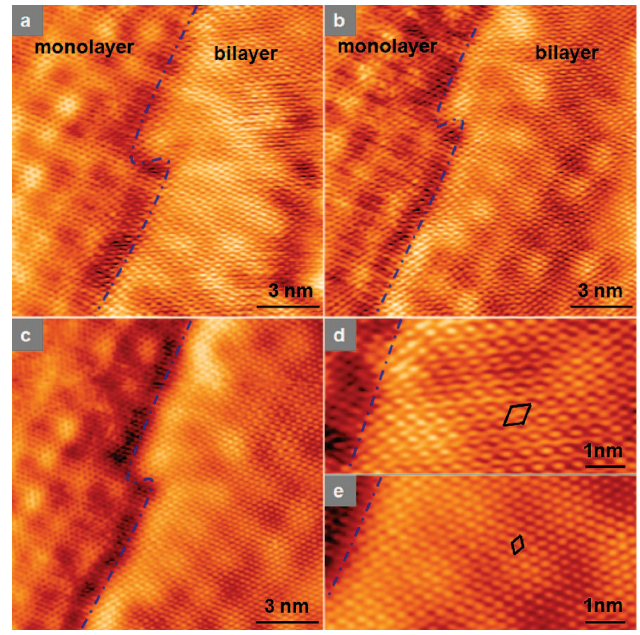

Figure 2. Bias dependent STM images (15×15 nm^2) at the domain boundaries between the monolayer and bilayer EG (the same region as marked by the black square in Figure 1a): (a) $V_T = 0.05$ V, (b) $V_T = -0.05$ V, and (c) $V_T = 0.1$ V. Panels d and e represent the corresponding detailed images (8×4 nm^2) of panels a and c, respectively. The diamonds in panels d and e highlight the ($\sqrt{3} \times \sqrt{3}$)*R*30° and 1×1 superstructure modulations observed on the bilayer EG regions, respectively.

Heating the SiC sample at higher temperature leads to the formation of trilayer EG. Figure 4a (80×60 nm^2,

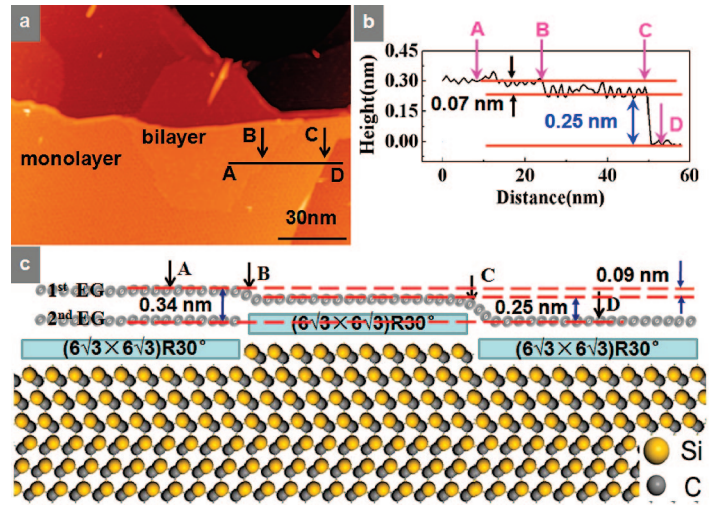

Figure 3. (a) Large scale STM image (150×100 nm^2, $V_T = 1.5$ V) showing the coexistence of the monolayer and bilayer EG. (b) Corresponding line profile measured along the black line AD marked in panel a. (c) Schematic of the proposed model revealing the atomic structures of the neighboring monolayer and bilayer EG on the same terrace, where the yellow circles represent Si atoms, gray circles for C atoms in bulk SiC and top light gray circles for C atoms in graphene.

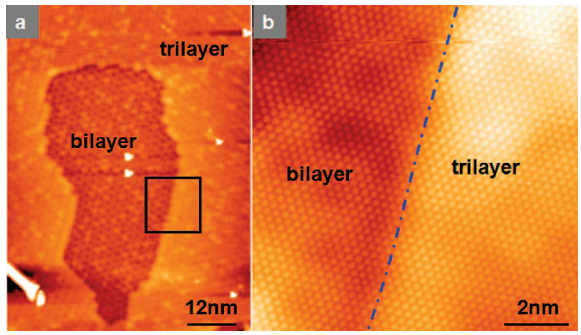

Figure 4. (a) Typical STM image (80 × 60 nm^2, V_T = 1.5 V) showing the coexistence of the bilayer (bright region) and trilayer (central dark region) EG on 6H-SiC(0001), and (b) its corresponding atomically resolved STM image (10 × 10 nm^2, V_T = 1.5 V) as marked by the square in panel a, revealing the physical continuum at the domain boundaries between the bilayer and trilayer EG.

V_T = 1.5 V) shows an STM image for the region covered by few layer EG with a depression at the image center. The 6 × 6 superstructure modulation from the underlying interfacial graphene is clearly observed in the depression but not in the surrounding bright regions. The corresponding high-resolution image in Figure 4b reveals that both the center depression and the surrounding bright regions possess the 1 × 1 triangular lattice typically observed on bilayer EG (*cf.* Figure 1b,d), suggesting that both regions are covered by EG with a thickness no less than two layers. Since the corrugation of the 6 × 6 superstructure in the depression is similar to that observed on bilayer EG, we assign the center depression as bilayer EG. Again, the top EG layer runs continuously from the center bilayer EG to the surrounding EG layer across the domain boundary, with the height difference measured to be about 0.07 nm. Therefore, we assign the EG on the surrounding bright region as trilayer EG. According to the bottom-up growth mode proposed above, the new interfacial graphene formed beneath the old interfacial graphene pushes up the bilayer EG by 0.07 nm, forming trilayer EG. This bottom-up growth ensures the continuity of the top EG layer from bilayer to trilayer EG.

CONCLUSION

In situ LT-STM has been used to study the epitaxial growth mechanism of EG on the 6H-SiC(0001). Atomic continuum at the domain boundaries transiting from monolayer to bilayer EG and from bilayer to trilayer EG has been observed, suggesting that the top EG layers on the same terrace originate from the same graphene layer. The height difference between monolayer and bilayer EG and bilayer and trilayer EG formed on the same terrace is measured to be 0.07 ± 0.01 nm, in good agreement with the value obtained by subtracting the SiC bilayer height (0.25 nm) from the EG interlayer spacing (0.34 nm). We propose a bottom-up growth mechanism to explain the 0.07 nm height difference and the physical continuum at the domain boundaries between monolayer, bilayer, and trilayer EG. This detailed understanding of epitaxial growth of EG on SiC has implications for the production of high quality and large scale EG films for their applications in graphene-based electronics.

METHODS

EG films were prepared by annealing chemically etched (10% HF solution) n-type Si-terminated 6H-SiC(0001) samples (CREE Research Inc.) at 850 °C under a silicon flux for 2 min in ultrahigh vacuum (UHV),[34,48] resulting in a Si-rich 3 × 3-reconstructed surface, and subsequently annealing the sample several times at a higher temperature (~1200 °C) in the absence of the silicon flux to form EG.[49−51] The thickness of EG films can be controlled by the annealing temperature and time followed by slow cooling to RT, allowing the preparation of samples with EG thicknesses ranging from one to three layers. The sample temperatures were measured by an optical pyrometer.

The *in situ* LT-STM experiments were carried out in a custom-built multichamber UHV system housing an Omicron LT-STM with base pressure better than 6.0 × 10^{-11} mbar.[52,53] All STM images were recorded in constant current mode using chemically etched tungsten (W) tips at 77 K. The low temperature used minimized thermal noise to give atomically resolved STM images, which were analyzed using WSxM software.[54]

Acknowledgment. We acknowledge the support from NRF-CRP grant "Graphene and Related Materials and Devices", the A*STAR grant R-398-000-036-305, and ARF grant R-144-000-196-112.

REFERENCES AND NOTES

1. Geim, A. K.; Novoselov, K. S. The Rise of Graphene. *Nat. Mater.* **2007**, *6*, 183–191.
2. Geim, A. K.; MacDonald, A. H. Graphene: Exploring Carbon Flatland. *Phys. Today* **2007**, *60*, 35–41.
3. Novoselov, K. S.; Geim, A. K.; Morozov, S. V.; Jiang, D.; Katsnelson, M. I.; Grigorieva, I. V.; Dubonos, S. V.; Firsov, A. A. Two-Dimensional Gas of Massless Dirac Fermions in Graphene. *Nature* **2005**, *438*, 197–200.
4. Novoselov, K. S.; Geim, A. K.; Morozov, S. V.; Jiang, D.; Zhang, Y.; Dubonos, S. V.; Grigorieva, I. V.; Firsov, A. A. Electric Field Effect in Atomically Thin Carbon Films. *Science* **2004**, *306*, 666–669.
5. Zhang, Y. B.; Tan, Y. W.; Stormer, H. L.; Kim, P. Experimental Observation of The Quantum Hall Effect and Berry's Phase in Graphene. *Nature* **2005**, *438*, 201–204.
6. Schedin, F.; Geim, A. K.; Morozov, S. V.; Hill, E. W.; Blake, P.; Katsnelson, M. I.; Novoselov, K. S. Detection of Individual Gas Molecules Adsorbed on Graphene. *Nat. Mater.* **2007**, *6*, 652–655.
7. Novoselov, K. S.; Jiang, Z.; Zhang, Y.; Morozov, S. V.; Stormer, H. L.; Zeitler, U.; Maan, J. C.; Boebinger, G. S.; Kim, P.; Geim, A. K. Room-Temperature Quantum Hall Effect in Graphene. *Science* **2007**, *315*, 1379.
8. Tombros, N.; Jozsa, C.; Popinciuc, M.; Jonkman, H. T.; van Wees, B. J. Electronic Spin Transport and Spin Precession in Single Graphene Layers at Room Temperature. *Nature* **2007**, *448*, 571–574.
9. Dresselhaus, M. S.; Dresselhaus, G. Intercalation Compounds of Graphite. *Adv. Phys.* **2002**, *51*, 1–186.
10. Li, X. L.; Wang, X. R.; Zhang, L.; Lee, S. W.; Dai, H. J. Chemically Derived, Ultrasmooth Graphene Nanoribbon Semiconductors. *Science* **2008**, *319*, 1229–1232.

11. Berger, C.; Song, Z. M.; Li, X. B.; Wu, X. S.; Brown, N.; Naud, C.; Mayou, D.; Li, T. B.; Hass, J.; Marchenkov, A. N. Electronic Confinement and Coherence in Patterned Epitaxial Graphene. *Science* **2006**, *312*, 1191–1196.
12. Berger, C.; Song, Z. M.; Li, X. B.; Ogbazghi, A. Y.; Dai, Z. T.; Marchenkov, A. N.; Conrad, E. H.; First, P. N.; de Heer, W. A. Ultrathin Epitaxial Graphite: 2D Electron Gas Properties and a Route toward Graphene-Based Nanoelectronics. *J. Phys. Chem. B* **2004**, *108*, 19912–19916.
13. Ferralis, N.; Maboudian, R.; Carraro, C. Evidence of Structural Strain in Epitaxial Graphene Layers on 6H-SiC(0001). *Phys. Rev. Lett.* **2008**, *101*, 156801-1–156801-4.
14. Emtsev, K. V.; Bostwick, A.; Horn, K.; Kellogg, G. L.; Ley, L.; McChesney, J. L.; Ohta, T.; Reshanov, S. A.; Rotenberg, E.; Schmid, A. K. *et al.* Atmospheric Pressure Graphitization of SiC(0001)—A Route towards Wafer-Size Graphene Layers. arXiv:0808.1222v1, arXiv.org e-Print archive; http://lanl.arxiv.org/abs/0808.1222, **2008**.
15. Dedkov, Y. S.; Fonin, M.; Ruediger, U.; Laubschat, C. Rashba Effect in the Graphene/Ni(111) System. *Phys. Rev. Lett.* **2008**, *100*, 107602-1–107602-4.
16. Nagashima, A.; Tejima, N.; Oshima, C. Electronic States of the Pristine and Alkali-Metal-Intercalated Monolayer Graphite/Ni(111) Systems. *Phys. Rev. B* **1994**, *50*, 17487–17495.
17. Dedkov, Y. S.; Shikin, A. M.; Adamchuk, V. K.; Molodtsov, S. L.; Laubschat, C.; Bauer, A.; Kaindl, G. Intercalation of Copper Underneath a Monolayer of Graphite on Ni(111). *Phys. Rev. B* **2001**, *64*, 035405-1–035405-6.
18. Coraux, J.; N'Diaye, A. T.; Busse, C.; Michely, T. Structural Coherency of Graphene on Ir(111). *Nano. Lett.* **2008**, *8*, 565–570.
19. N'Diaye, A. T.; Bleikamp, S.; Feibelman, P. J.; Michely, T. Two-Dimensional Ir Cluster Lattice on a Graphene Moire on Ir(111). *Phys. Rev. Lett.* **2006**, *97*, 215501-1–215501-4.
20. Sutter, P. W.; Flege, J.; Sutter, E. A. Epitaxial Graphene on Ruthenium. *Nat. Mater.* **2008**, *7*, 406–411.
21. Marchini, S.; Gunther, S.; Wintterlin, J. Scanning Tunneling Microscopy of Graphene on Ru(0001). *Phys. Rev. B* **2007**, *76*, 075429-1–075429-9.
22. Wu, Y. Q.; Ye, P. D.; Capano, M. A.; Xuan, Y.; Sui, Y.; Qi, M.; Cooper, J. A.; Shen, T.; Pandey, D.; Prakash, G. Top-Gated Graphene Field-Effect-Transistors Formed by Decomposition of SiC. *Appl. Phys. Lett.* **2008**, *92*, 092102-1–092102-3.
23. Bolotin, K. I.; Sikes, K. J.; Jiang, Z.; Klima, M.; Fudenberg, G.; Hone, J.; Kim, P.; Stormer, H. L. Ultrahigh Electron Mobility in Suspended Graphene. *Solid State Commun.* **2008**, *146*, 351–355.
24. Du, X.; Skachko, I.; Barker, A.; Andrei, E. Y. Approaching Ballistic Transport in Suspended Graphene. *Nat. Nanotechnol.* **2008**, *3*, 491–495.
25. van Bommel, A. J.; Crombeen, J. E.; van Tooren, A. LEED and Auger Electron Observation of the SiC(0001) Surface. *Surf. Sci.* **1975**, *48*, 463–472.
26. Johansson, L. I.; Owman, F.; Martensson, P. High-Resolution Core-Level Study of 6H-SiC(0001). *Phys. Rev. B* **1996**, *53*, 13793–13802.
27. Owman, F.; Matrensson, P. The SiC(0001) $6\sqrt{3} \times 6\sqrt{3}$ Reconstruction Studied with STM and LEED. *Surf. Sci.* **1996**, *369*, 126–136.
28. Forbeaux, I.; Themlin, J. M.; Debever, J. M. Heteroepitaxial Graphite on 6H-SiC(0001): Interface Formation through Conduction-Band Electronic Structure. *Phys. Rev. B* **1998**, *58*, 16396–16406.
29. Mattausch, A.; Pankratov, O. *Ab Initio* Study of Graphene on SiC. *Phys. Rev. Lett.* **2007**, *99*, 076802-1–076802-4.
30. Kim, S.; Ihm, J.; Choi, H. J.; Son, Y. W. Origin of Anomalous Electronic Structures of Epitaxial Graphene on Silicon Carbide. *Phys. Rev. Lett.* **2008**, *100*, 176802-1–176802-4.
31. Kusunoki, M.; Suzuki, T.; Hirayama, T.; Shibata, N.; Kaneko, K. A Formation Mechanism of Carbon Nanotube Films on SiC(0001). *Appl. Phys. Lett.* **2000**, *77*, 531–533.
32. Wang, Z.; Irle, S.; Zheng, G. S.; Kusunoki, M.; Morokuma, K. Carbon Nanotubes Grow on the C Face of SiC(000−1) during Sublimation Decoposition: Quantum Chenical Molecular Dynamics Simulations. *J. Phys. Chem. C* **2007**, *111*, 12960–12972.
33. Goknur Cambaz, Z.; Yushin, G.; Osswald, S.; Mochalin, V.; Gogotsi, Y. Noncatalytic Synthesis of Carbon Nanotubes, Graphene and Graphite on SiC. *Carbon* **2008**, *46*, 841–849.
34. Chen, W.; Xu, H.; Liu, L.; Gao, X. Y.; Qi, D. C.; Peng, G. W.; Tan, S. C.; Feng, Y. P.; Loh, K. P.; Wee, A. T. S. Atomic Structure of the 6H-SiC(0001) Nanomesh. *Surf. Sci.* **2005**, *596*, 176–186.
35. Riedl, C.; Starke, U.; Bernhardt, J.; Franke, M.; Heinz, K. Structural Properties of the Graphene-SiC(0001) Interface as a Key for the Preparation of Homogeneous Large-Terrace Graphene Surfaces. *Phys. Rev. B* **2007**, *76*, 245406-1–245406-8.
36. Lauffer, P.; Emtsev, K. V.; Graupner, R.; Seyller, Th.; Ley, L.; Reshanov, S. A.; Weber, H. B. Atomic and Electronic Structure of Few-Layer Graphene on SiC(0001) Studied with Scanning Tunneling Microscopy and Spectroscopy. *Phys. Rev. B* **2008**, *77*, 155426-1–155426-10.
37. Brar, V. W.; Zhang, Y. B.; Yayon, Y.; Ohta, T.; McChesney, J. L.; Bostwick, A.; Rotenberg, E.; Horn, K.; Crommie, M. F. Scanning Tunneling Spectroscopy of Inhomogeneous Electronic Structure in Monolayer and Bilayer Graphene on SiC. *Appl. Phys. Lett.* **2007**, *91*, 122102-1–122102-3.
38. Filleter, T.; Emtsev, K. V.; Seyller, Th.; Bennewitz, R. Local Work Function Measurements of Epitaxial Graphene. *Appl. Phys. Lett.* **2008**, *93*, 133117-1–133117-3.
39. Tomanek, D.; Louie, S. G.; Mamin, H. J.; Abraham, D. W.; Thomsom, R. E.; Ganz, E.; Clarke, J. Theory and Observation of Highly Asymmetric Atomic-Structure in Scanning Tunneling Microscopy Imanges of Graphite. *Phys. Rev. B* **1987**, *35*, 7790–7793.
40. Yang, H.; Baffou, G.; Mayne, A. J.; Comtet, G.; Dujardin, G.; Kuk, Y. Topology and Electron Scattering Properties of the Electronic Interfaces in Epitaxial Graphene Probed by Resonant Tunneling Spectroscopy. *Phys. Rev. B* **2008**, *78*, 041408-1–041408-4.
41. Charrier, A.; Coati, A.; Argunova, T.; Thibaudau, F.; Garreau, Y; Pinchaux, R.; Forbeaux, I.; Debever, J. M.; Sauvage-Simkin, M.; Themlin, J. M. Solid-State Decomposition of Silicon Carbide for Growing Ultra-Thin Heteroepitaxial Graphite Films. *J. Appl. Phys.* **2002**, *92*, 2479–2484.
42. Rutter, G. M.; Guisinger, N. P.; Crain, J. N. N.; Jarvis, E. A. A.; Stiles, M. D.; Li, T.; First, P. N.; Stroscip, J. A. Imaging the Interface of Epitaxial Graphene with Silicon Carbide *via* Scanning Tunneling Microscopy. *Phys. Rev. B* **2007**, *76*, 235416-1–235416-6.
43. Rutter, G. M.; Crain, J. N.; Guisinger, N. P.; Li, T.; First, P. N.; Stroscio, J. A. Scattering and Interference in Epitaxial Graphene. *Science* **2007**, *317*, 219–222.
44. Mizes, H. A.; Foster, J. S. Long-Rang Electronic Perturbations Caused by Defects Using Scanning Tunneling Microscopy. *Science* **1989**, *244*, 559–562.
45. Tapaszto, L.; Dobrik, G.; Lambin, P.; Biro, L. P. Tailoring the Atomic Structure of Graphene Nanoribbons by Scanning Tunnelling Microscope Lithography. *Nat. Nanotechnol.* **2008**, *3*, 397–401.
46. Varchon, F.; Feng, R.; Hass, J.; Li, X.; Nguyen, B. N.; Naud, C.; Mallet, P.; Veuillen, J. Y.; Berger, C.; Conrad, E. Electronic Structure of Epitaxial Graphene Layers on SiC: Effect of the Substrate. *Phys. Rev. Lett.* **2007**, *99*, 126805-1–126805-4.
47. Gao, X. Y.; Chen, S.; Liu, T.; Chen, W.; Wee, A. T. S.; Nomoto, T.; Yagi, S.; Yuhara, J. Disorder beneath Epitaxial Graphene on SiC(0001): An X-ray Absorption Study. *Phys. Rev. B* **2008**, *78*, 202404(R)-1–202404(R)-4.
48. Poon, S. W.; Chen, W.; Tok, E. S.; Wee, A. T. S. Probing Epitaxial Growth of Graphene on Silicon Carbide by Metal Decoration. *Appl. Phys. Lett.* **2008**, *92*, 104102-1–104102-3.
49. Forbeaux, I.; Themlin, J. M.; Debever, J. M. High-Temperature Graphitization of the 6H-SiC (000−1) Face. *Surf. Sci.* **1999**, *442*, 9–18.

50. Mallet, P.; Varchon, F.; Naud, C.; Magaud, L.; Berger, C.; Veuillen, J. Y. Electron States of Mono- and Bilayer Graphene on SiC Probed by Scanning-Tunneling Microscopy. *Phys. Rev. B* **2007**, *76*, 041403-1–041403-4.
51. Bostwick, A.; Ohta, T.; Seyller, Th.; Horn, K.; Rotenberge, E. Quasiparticle Dynamics in Graphene. *Nat. Phys.* **2007**, *3*, 36–40.
52. Zhang, H. L.; Chen, W.; Chen, L.; Huang, H.; Wang, X. S.; Yuhara, J.; Wee, A. T. S. C_{60} Molecular Chains on *a*-Sexthiophene Nanostripes. *Small* **2007**, *3*, 2015–2018.
53. Huang, H.; Chen, W.; Wee, A. T. S. Low-Temperature Scanning Tunneling Microscopy Investigation of Epitaxial Growth of F_{16}CuPc Thin Films on Ag(111). *J. Phys. Chem. C* **2008**, *112*, 14913–14918.
54. Horcas, I.; Fernandez, R.; Gomez-Rodriguez, J. M. M.; Colchero, J. WSXM: A Software for Scanning Probe Microscopy and a Tool for Nanotechnology. *Rev. Sci. Instrum.* **2007**, *78*, 013705-1–013705-8.